The role of arginine 143 in the electrostatics and mechanism of Cu, Zn superoxide dismutase: Computational and experimental evaluation by mutational analysis

ARTICLE *in* PROTEINS STRUCTURE FUNCTION AND BIOINFORMATICS · MAY 1994

Impact Factor: 2.63 · DOI: 10.1002/prot.340190105

5 AUTHORS, INCLUDING:

Diane E Cabelli
Brookhaven National Laboratory
99 PUBLICATIONS **3,128** CITATIONS
SEE PROFILE

John Tainer
University of Texas MD Anderson Cancer Center
457 PUBLICATIONS **30,025** CITATIONS
SEE PROFILE

PROTEINS: Structure, Function, and Genetics 19:24–34 (1994)

The Role of Arginine 143 in the Electrostatics and Mechanism of Cu,Zn Superoxide Dismutase: Computational and Experimental Evaluation by Mutational Analysis

Cindy L. Fisher,[1] Diane E. Cabelli,[2] John A. Tainer,[1] Robert A. Hallewell,[3] and Elizabeth D. Getzoff[1]
[1]Department of Molecular Biology, The Scripps Research Institute, La Jolla, California, 92037, [2]Department of Chemistry, Brookhaven National Laboratory, Upton, Long Island, New York 11973, and [3]Department of Biochemistry, Imperial College, London, SW7 2AZ, U.K.

ABSTRACT **Cu,Zn superoxide dismutase protects cells from oxidative damage by removing superoxide radicals in one of the fastest enzyme reactions known. The redox reaction at the active-site Cu ion is rate-limited by diffusion and enhanced by electrostatic guidance. To quantitatively define the electrostatic and mechanistic contributions of sequence-invariant Arg-143 in human Cu,Zn superoxide dismutase, single-site mutants at this position were investigated experimentally and computationally. Rate constants for several Arg-143 mutants were determined at different pH and ionic strength conditions using pulse radiolytic methods and compared to results from Brownian dynamics simulations. At physiological pH, substitution of Arg-143 by Lys caused a 2-fold drop in rate, neutral substitutions (Ile, Ala) reduced the rate about 10-fold, while charge-reversing substitutions (Asp, Glu) caused a 100-fold decrease. Position 143 mutants showed pH dependencies not seen in other mutants. At low pH, the acidic residue mutations exhibited protonation/deprotonation effects. At high pH, all enzymes showed typical decreases in rate except the Lys mutant in which the rate dropped off at an unusually low pH. Increasing ionic strength at acidic pH decreased the rates of the wild-type enzyme and Lys mutant, while the rate of the Glu mutant was unaffected. Increasing ionic strength at higher pH (>10) increased the rates of the Lys and Glu mutants while the rate of the wild-type enzyme was unaffected. Reaction simulations with Brownian dynamics incorporating electrostatic effects tested computational predictability of ionic strength dependencies of the wild-type enzyme and the Lys, Ile, and Glu mutants. The calculated and experimental ionic strength profiles gave similar slopes in all but the Glu mutant, indicating that the electrostatic attraction of the substrate is accurately modeled. Differences between the calculated and experimental rates for the Glu and Lys mutants reflect the mechanistic contribution of Arg-143. Results from this joint analysis establish that, aside from the Cu ligands, Arg-143 is the single most important residue in Cu,Zn superoxide dismutase both electrostatically and mechanistically, and provide an explanation for the evolutionary selection of arginine at position 143.** © 1994 Wiley-Liss, Inc.

Key words: Brownian dynamics, molecular recognition, site-directed mutagenesis, facilitated diffusion

INTRODUCTION

The intracellular Cu,Zn superoxide dismutases (SODs) are predominantly found in the cytosol and peroxisomes of eukaryotes[1,2] and protect these cells from the toxic effects of the superoxide radical produced as a byproduct of aerobic metabolism.[3] This protection is critical biologically, as evidenced from recent studies that link single-site SOD mutants to the fatal paralytic disorder amyotrophic lateral sclerosis (ALS), otherwise known as Charcot's or Lou Gehrig's disease.[4,5] The role of individual residues in the enzyme's activity has been shown to be relevant both scientifically and medically.

Cu,Zn SOD is a homodimer consisting of about 153 amino acids and containing one copper and one zinc ion per subunit.[6] The copper ion is an essential cofactor in catalysis and is cyclically oxidized and reduced during successive encounters with the negatively charged superoxide radical. The dismutation of superoxide radicals yielding molecular oxygen and hydrogen peroxide is rapid ($V_{max} \sim 2 \times 10^9\ M^{-1}\ s^{-1}$).[7,8] The rate is diffusion-limited, as demonstrated experimentally by decreasing the reaction

Received September 23, 1993; revision accepted December 3, 1993.

Address reprint requests to Elizabeth D. Getzoff, The Scripps Research Institute, Department of Molecular Biology—MB4, 10666 North Torrey Pines Road, La Jolla, CA 92037.

rate when increasing solution viscosity,[7] and is facilitated by local electrostatic forces, as seen from the enzyme's ionic strength dependence.[9–12]

Analysis of the X-ray structure of bovine SOD revealed that an Arg residue (Arg-143 in human SOD) is located adjacent to the active site copper ion.[13,14] Chemical modification[15–18] and site-directed mutagenesis[19] studies showed the importance of Arg-143 for catalysis. Arg-143 also forms part of the peroxisomal targeting signal of the enzyme.[1] This residue was identified as invariant in SOD[20] and remains invariant among the 40 SODs sequenced thus far (unpublished compilation by E.D.G., J.A.T., R.A.H., and R.J. Peters). Computer graphic and computational analysis of the electrostatic potential around the active site predicts that the Arg residue is important for short-range electrostatic attraction of the negatively charged substrate.[21]

We report here a combined experimental and theoretical investigation of mutants of human SOD, in which the Arg residue at position 143 has been replaced with the less diffuse positive charge of a Lys (R143K), the neutral groups of either an Ile (R143I) or an Ala (R143A), and the negatively charged groups of Asp (R143D) or Glu (R143E). Rates measured experimentally by pulse radiolysis are compared with those calculated from Brownian dynamics simulations incorporating electrostatic effects to differentiate the electrostatic and mechanistic roles of Arg-143 in the enzyme's activity.

METHODS

Site-Directed Mutants

The wild-type enzyme and R143I, R143A, and R143K mutants were made in a yeast expression system in which M13 site-directed mutagenesis using mutagenic oligonucleotide primers introduced mutations into the human SOD cDNA as described previously.[19] After transformation and sequencing of the mutant clones, *Nco*I–*Sal*I restriction fragments of mutant double-stranded M13 DNA were cloned into the yeast expression plasmid pC1/1PGAPSOD and expressed in yeast strain AB110 Leu$^-$ under the control of the glyceraldehyde phosphate dehydrogenase gene 49 promoter.

The R143D and R143E proteins were made by periplasmic expression in an *Escherichia coli* strain lacking any endogenous SODs using the pPHSOD1LacI^q plasmid as described previously.[22] The low activity of the R143D and R143E enzymes necessitated this switch from the yeast to the *E. coli* system to avoid possible copurification of the small amount of heterodimeric enzyme formed between the fully active endogenous yeast Cu,Zn SOD and the mutant human enzyme. In pPHSOD1LacI^q, a synthetic human SOD gene incorporating the Cys 6→Ala and Cys 111→Ser thermostable mutations[23,24] is joined to the leader sequence of *Photobacterium leiognathi* SOD[25] and the *lacI^q* gene[26] and placed under the control of the *tac1* promoter.[27] This thermostable mutant maintains the activity, rate-versus-pH profile, and active site structure[6,24,28] of wild-type human SOD. Mutants were made by substituting double-stranded synthetic oligonucleotides between the unique *Spe*I and *Bam*HI sites in pPHSOD1LacI^q. Processing occurred correctly using the *P. leiognathi* signal peptide to leave an N-terminal alanine. The DNA encoding each mutant gene was sequenced in its entirety to ensure no other amino acid changes were present.

Recombinant human SOD proteins were produced in *E. coli* at about 10% of total cellular protein after overnight induction of the *tac1* promoter with 0.2 mM isopropyl-β-D-thiogalactopyranoside in 10 liters of L-broth containing 100 μg ml^{-1} ampicillin and 0.1 mM $CuSO_4$.[27] The periplasmic human[22] SOD proteins were purified to ~95% homogeneity by heating at 65°C for 2 hr, followed by DEAE-Sepharose chromatography.[19] All proteins were dialyzed against 20 mM Tris buffer at pH 8 with 1 mM $CuSO_4$, then extensively against water. Protein concentrations were determined spectrophotometrically at 265 nm and by dry weight measurements.[19]

Experimental Rate Measurements

The reaction rates of human SOD and the mutants of Arg-143 reported here were measured in pulse radiolytic experiments carried out with the 2-MeV van de Graaff generator at Brookhaven National Laboratories as described previously.[29] Superoxide radicals were generated at radiation doses of 150–2000 rads (yielding 1–20 μmol of superoxide) in air/oxygen-saturated aqueous solutions[30] containing 10 mM sodium formate (Sigma Chemical Co.) and water that was purified by distillation followed by filtration through a Millipore ultrapurification system. Any adventitious metal ions present in the solution that might dismute superoxide and skew results were scavenged by the addition of 50–130 μM diethylenetetraminepentaacetate (DTPA, Sigma) or 70–80 μM ethylenediaminetetraacetic acid (EDTA, Sigma). Either *N*-[2-hydroxyethyl]piperazine-*N'*-[2-ethanesulfonic acid] (HEPES, 0.5 mM, Sigma) or sodium dihydrogen phosphate (1–10 mM, Ultrex, J. T. Baker, Inc.) was usually added as a buffering agent. The pH dependency of rate was measured both with phosphate and with HEPES as buffers to test for possible binding of phosphate anion at the active site, which probably occurs when Glu 133 is mutated to Gln.[22] No significant differences in rate were seen between the two buffers. If phosphate did bind at the active sites of any of these enzymes, it did not affect reaction rates.

Atomic absorption spectroscopy was used to determine the level of activity-essential copper present and thus the concentration of active enzyme. Decay of superoxide was monitored spectrophotometrically at 245–270 nm in the presence of 1–10 μM

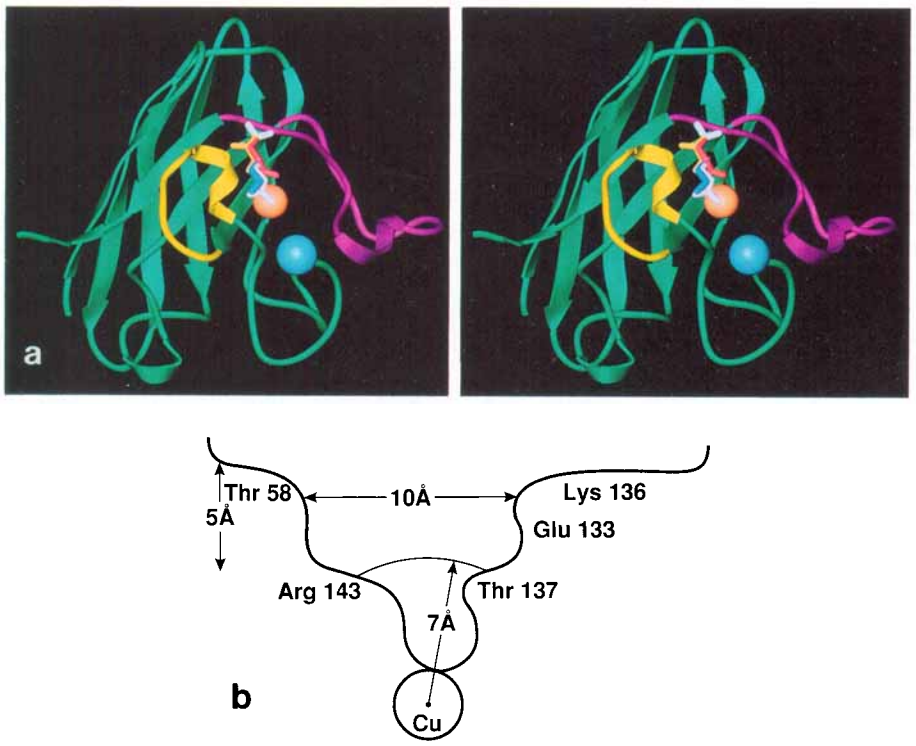

Fig. 1. **(a)** SOD subunit fold, active site metal ions, and relative positions of side chains at position 143 in wild-type X-ray crystal structure and models of mutants. The protein backbone is indicated by the green ribbon, with the electrostatic loop colored magenta and the disulfide loop colored gold. The wild-type Arg side chain is shown in white, that of the Lys mutant in blue, that of the Ile mutant in yellow and that of the Glu mutant in red. The copper and zinc ion positions are indicated by the orange and blue spheres, respectively. Figure constructed using the program Ribbons[40] converted by A. Shah for rendering with AVS.[41] **(b)** A schematic representation of the cross-section of the active site channel of SOD, showing its shape, dimensions, and the approximate location of the side chains that form it. The arc shows the 7Å reaction radius used for counting productive collisions of superoxide in the Brownian dynamics simulations (see "Methods").

O_2^- and 1–10 μM SOD. As SOD is dimeric in vivo, catalytic rates were calculated from the active enzyme concentrations determined by halving the copper ion concentrations measured with atomic absorption spectroscopy (Pye-Unicam or GBC instrument). This adjustment gives the rate per dimer.

For the ionic strength dependency studies, sodium chloride in concentrations of 0.008 to 0.25 M (Ultrex, J. T. Baker, Inc.) was added to the solutions. For the pH dependency studies, the pH was adjusted by either NaOH (99.999% pure, GFS Chemicals) or H_2SO_4 (Aristar, BDH Chemical Co.). The enzymes were not deactivated over the pH ranges used, as measurements on each SOD solution began at neutral pH, continued to one pH extreme, reversed to the other extreme, and were then brought back to neutrality again with no significant loss in activity.

Electrostatic Calculations and Brownian Dynamics Simulations

Polar (nitrogen and oxygen) atoms of one of the five dimers in the three-dimensional X-ray structural coordinates of the human (Cys 6→Ala, Cys 111→Ser) SOD[6] were protonated with the program InsightII (Biosym Technologies, Inc., San Diego, CA). Structures of the mutants R143K, R143I, and R143E were generated by replacing the Arg with the appropriate residue within InsightII and energy-minimizing the resulting coordinates with Discover (Biosym Technologies, Inc.) on a Convex C240 minisupercomputer by holding all atoms but those in the mutated residue fixed. First, the steepest descents algorithm was used, ignoring Morse potential and cross terms, until the maximum potential energy derivative was lower than 1.0 kcal mol^{-1} $Å^{-1}$. The conjugate gradients algorithm was then applied, including Morse potential and cross terms, until the maximum derivative was less than 1×10^{-3} kcal mol^{-1} $Å^{-1}$. The resultant structures are all stereochemically reasonable and assume no gross rearrangements upon mutation (see Fig. 1). During the minimization, the negatively charged glutamic acid side chain of the R143E enzyme moved closer to the copper, as also seen in molecular dynamics simulations of the mutant.[31]

Electrostatic potentials around the four proteins were calculated with version 2.1.1 of the University of Houston Brownian Dynamics (UHBD) program

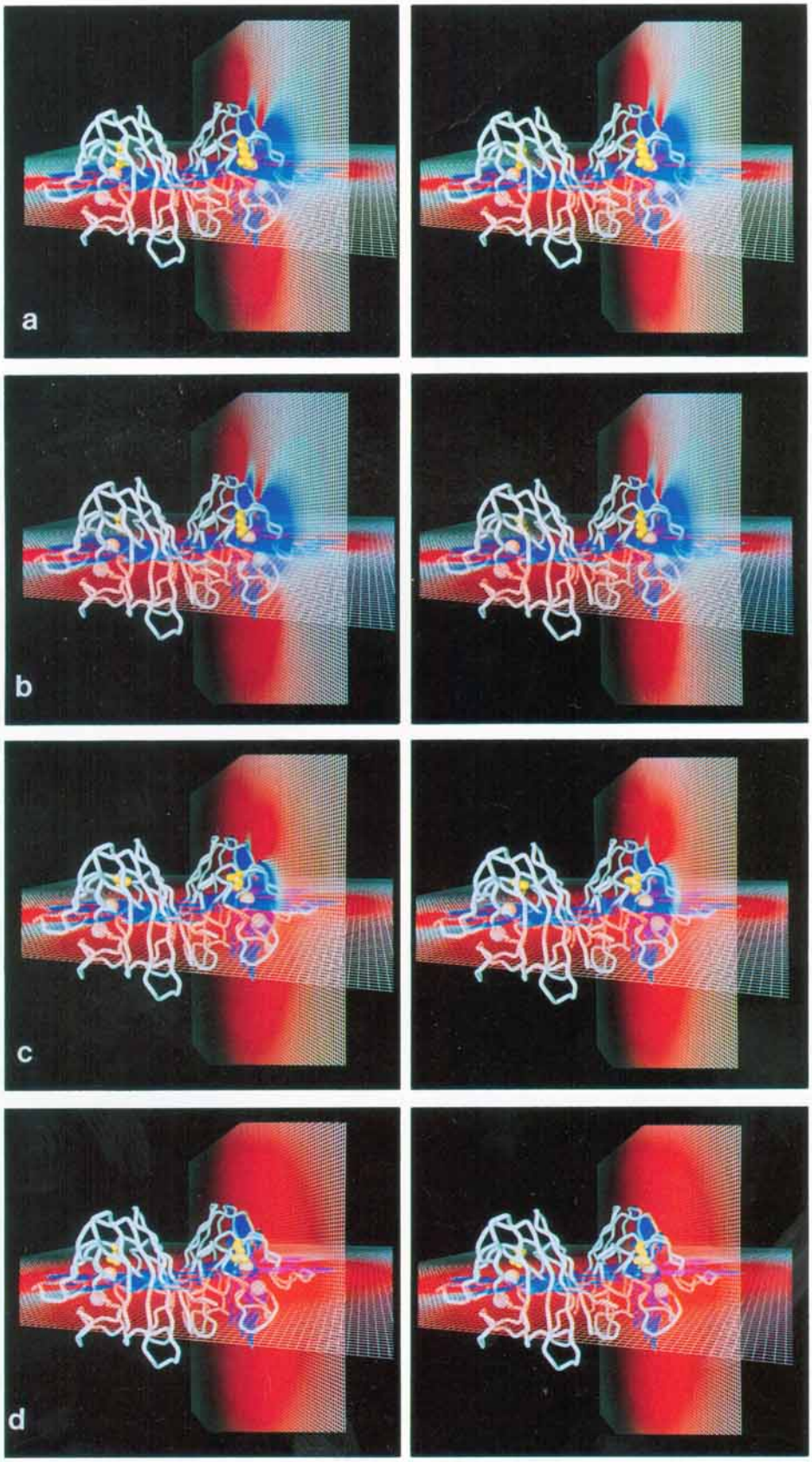

Fig. 2. Slices through the electrostatic potential grids of **(a)** the wild-type SOD dimer, **(b)** the R143K mutant, **(c)** the R143I mutant, and **(d)** the R143E mutant. The slices pass through the copper ions at the bottom of the active site channels of both dimers. Positive potential is indicated in blue, negative in red. The color changes on the vertical plane highlight the decrease in attractive positive potential (blue) around the active site upon charge neutralization (c) and reversal (d) of Arg-143. The overall net negative charge on wild-type and mutant SODs leads to the dominance of negative potential (red). Cα traces of SOD dimer backbones indicated by white tubes, copper and zinc ion positions by the orange and blue spheres, respectively, and the residue at position 143 by large yellow tubes. Figure rendered with the program AVS,[41] with tubes generated by the module MCS TUBES (written by Y. Chen and A. Olson).

developed by J. D. Madura and M. E. Davis in collaboration with J. A. McCammon,[32] running on a Convex C240, the Cray Y-MP4E at Scripps, a Cray Y-MP8E at Cray Research, Inc., and several Sun Sparcstations. The program determines the electrostatic forces from the linearized Poisson–Boltzmann equation at points on a grid around the protein. In this work, a grid was constructed with 128 × 128 × 128 points at a spacing of 1 Å and centered at the geometric center of the protein dimer. Grid points were assigned a dielectric constant of 2 inside the protein and a value of 78 outside the protein. Protein atoms were treated as discrete points with partial charges from AMBER,[33] assuming a pH of 7, and radii[34] assigned following guidelines described previously.[21] The potential at the grid boundary was calculated using Debye–Hückel theory, assuming the protein was a finite sphere of radius 30.0 Å with a net charge equivalent to that of the protein under study, and a boundary smoothing function applied. At Scripps, the original UHBD program was modified to allow standard radii[34] to be used for calculating the protein/solvent boundaries in both collision detection and the electrostatic grid calculation. In this work, standard radii[34] were used for all atomic radii, i.e., no adjustments were made in the active site cavity since they were found to be unnecessary with the present parameter set and program. Electrostatic potential values were calculated at the grid points (see Fig. 2), converging the total electrostatic potential to a deviation of $< 10^{-8}$ between iterations for the wild-type and each mutant at four different ionic strengths: 0.025, 0.075, 0.150, and 0.260 M.

Brownian dynamics simulations were run with most parameters assigned as described by Sines et al.[11] and our previous work.[22] The hydrodynamic radii of the superoxide molecule and SOD dimer were assumed to be 2.05 and 28.5 Å, respectively, and the slip hydrodynamic boundary condition was used. Superoxide molecules were modeled as single points. To calculate trajectories, each superoxide was started at a random location on a sphere 41.5 Å from the geometric center of SOD, and moved under the influence of the protein's electrostatic force. (Tests using a 60.0-Å sphere gave essentially the same results.) Trajectories were pursued until the superoxide exited the system, bounded at 500 Å from the center of the protein, or until reaction occurred.[11] The time between steps in each trajectory varied with distance from the protein center: 0.01 psec within 40 Å, 0.25 psec between 40 and 100 Å, and 1.0 psec beyond 100 Å. Reaction was defined as approach of superoxide to within 7.0 Å of the copper ion (see arc in Fig. 1b) in either of the two subunits. The reaction rate was calculated from the probability of reaction determined from the ratio of the number of collisions to the total number of trajectories. Each computational data point in Figure 4 represents the simulation of 12,000 or more trajectories, resulting in 90% confidence level variations of less than 10%.

Collisions of the superoxide with other parts of the protein were detected by an exclusion grid. Since the reactant species, superoxide, is treated as a point by the UHBD program, the program was modified to allow expansion of each protein atom's van der Waals radius by an additive adjustment factor to define the exclusion volume. In this work, an adjustment of 1.5 Å was used, mimicking an oxygen radius.

RESULTS AND DISCUSSION

Residue 143: Structural Overview and Charge/Activity Relationships

Arg-143 lies in an extended loop at the beginning of the C-terminal β-strand. Its extended side chain packs against the outside of the β-barrel and projects outward into the active site channel between the two large loops (loops IV and VII) that form the channel.[6,20] The Arg-143 main-chain position is highly restrained by main-chain β-bulge hydrogen bonds to adjacent residues 142 and 144. Although solvent-exposed, its side chain is sterically constrained, being sandwiched between His-48 (one of the copper ligands) and Thr-58 from the disulfide subloop of loop IV. Due to these tight structural restrictions, the replacement side chains at position 143 in the energy-minimized model structures for the mutants R143K, R143I, and R143E (Fig. 1a) had the same general conformation as the Arg, consistent with initial x-ray structural results on the R143I mutant (H. E. Parge, R.A.H., J.A.T., unpublished results). The mutated side chains did not collide or interact unfavorably with the rest of the protein, and appeared reasonable and sufficiently accurate for the purposes of electrostatic calculations and Brownian dynamics simulations.

The Arg-143 side chain, which forms one rim of the active site channel directly above the copper ion (Fig. 1), can contribute both mechanistically and electrostatically to the enzyme rate. The electrostatics and Brownian dynamics calculations provide direct information only on the electrostatic role of Arg-143 in facilitated diffusion (Fig. 2), but cannot provide information about its mechanistic role. Experimental results demonstrate the effects of both. In tandem, experimental and computational results define the electrostatic contributions and estimate the specific mechanistic contributions of Arg-143 to the enzymatic rate.

Mutation of Arg-143 in human SOD to Lys, Ile, Ala, Asp, or Glu resulted in enzymes of lower activities, as determined experimentally from reaction rates measured by pulse radiolysis. At physiological pH, the wild-type SOD had the highest rate, the R143K mutant rate dropped by a factor of 2, the R143I and R143A mutants by an order of magni-

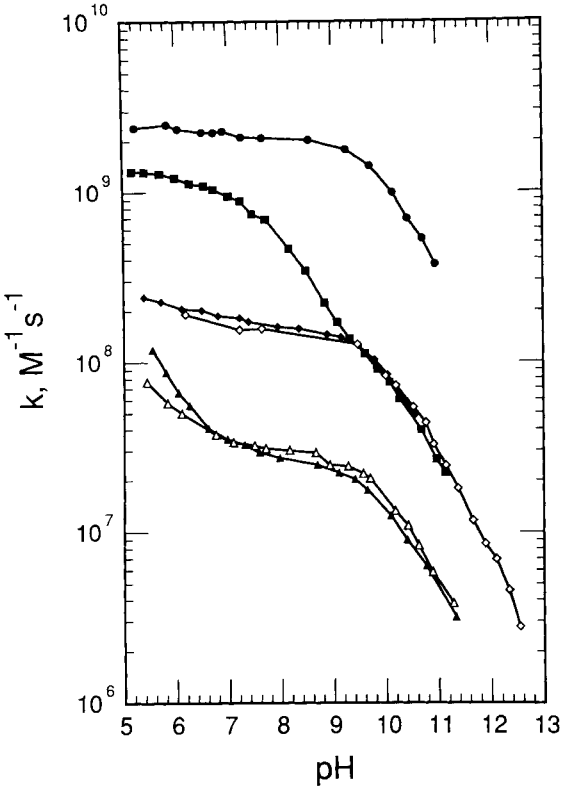

Fig. 3. Reaction rate dependence on pH for wild-type and mutant enzymes. At pH 8, the wild-type enzyme (●) had the highest activity followed by mutant R143K (■); mutants R143I (◆) and R143A (◇) had intermediate rates, and R143E (▲) and R143D (△) the lowest. Data were obtained in solutions of 0.5 mM HEPES and 0.01M sodium formate, except R143A where 1 mM sodium dihydrogen phosphate was used instead of HEPES. In most cases, 72 μM EDTA was added to chelate any free copper ions; in the wild-type and R143A enzymes 50–130 μM DTPA was used instead. Concentrations of SOD varied from 1.124 to 8.28 μM.

tude, and the R143D and R143E mutants by almost two orders of magnitude (Fig. 3). Thus, loss of a positive charge at position 143 was detrimental to enzyme function, and charge reversal even more so. Charge alteration at this position has had the most dramatic effect on enzymatic activity of any mutant studied thus far[22] (E.D.G., R.A.H., J.A.T., D.E.C., unpublished results). These relative rates generally agree with activity measurements obtained by xanthine oxidase/cytochrome *c* methods at pH 7.8—wild-type 100%, R143K 43.2%, and R143I, 10.8%.[19] This trend also corroborates the azide affinity results found by Banci et al.[36]

pH Profiles of Enzyme Rates

Plots of pH versus rate indicate titration of residues critical to the activity and can reveal shifts in or additional mutant pK_a values relative to the wild-type protein. Most SOD mutants studied to date have enzymatic rates with a pH dependency pattern similar to that of the wild-type enzyme: a near-constant rate from pH 5–8, with a sharp drop at higher pH due to deprotonation events in other areas of the protein and/or difficulty in protonating superoxide as the overall negative charge of the enzyme increases. Among the 143 mutants, however, only the charge-neutralization mutants R143I and R143A demonstrated this behavior (Fig. 3), indicative of a unique pH dependency in this residue.

In the two charge-reversal mutants, R143D and R143E, rates increased sharply at low pH due to reversible protonation of the introduced carboxylic acid. Thus at low pH (typical p*K*s of unsequestered carboxylate moieties of Asp and Glu are 3.9 and 4.3, respectively), the extra negative charge created at the active site by these was eliminated. Near pH 5 the increased concentration of neutralized enzyme resulted in an activity approaching that of uncharged mutants R143I and R143A.

The R143K mutant exhibited an unusual drop in rate as the pH increased, starting at pH 7 (Fig. 3) and fully reversible with pH, which can be attributed to neutralization by deprotonation of the amino group of the Lys side chain (typical p*K* for the amino group of Lys is 10.8). This interpretation is supported by the fact that the deprotonation processes in the R143D and R143E mutants exhibited a drop of equivalent magnitude (about 5-fold) at low pH. At pH 9.5 the activity of deprotonated R143K enzyme is equivalent to that of the uncharged R143I and R143A mutants.

The results of pH dependence in the wild-type and mutant enzyme rates demonstrate that an Arg at position 143 is critical in keeping a stable, strong, positive charge at the active site to pHs up to 10. Even substitution with Lys is insufficient to maintain positive charge dominance much above pH 7.

Experimental and Calculated Ionic Strength Dependencies of Enzyme Rates

The ionic strength dependence reflects the involvement of local and global electrostatic guidance of the negatively charged superoxide substrate by the enzyme. The formal charges of superoxide (−1) and SOD enzyme overall (−4 to −8 in the dimeric systems studied here) are both negative. If global electrostatic forces dominate the SOD–superoxide interaction, increasing the ionic strength of the intervening solution should decrease the electrostatic repulsion, thus increasing the reaction rate. If positive charges local to the active site dominate, both the resulting attractive electrostatic interaction and the enzymatic rate would decrease with increasing ionic strength. Pulse radiolysis measurements at pH 8 show that the latter applies in the wild-type enzyme.[22]

In Figure 4, the ionic strength dependence of the enzymatic rate is assessed by plotting the log of the observed second-order rate constant (k) as a function of the square root of ionic strength ($I^{1/2}$) for the na-

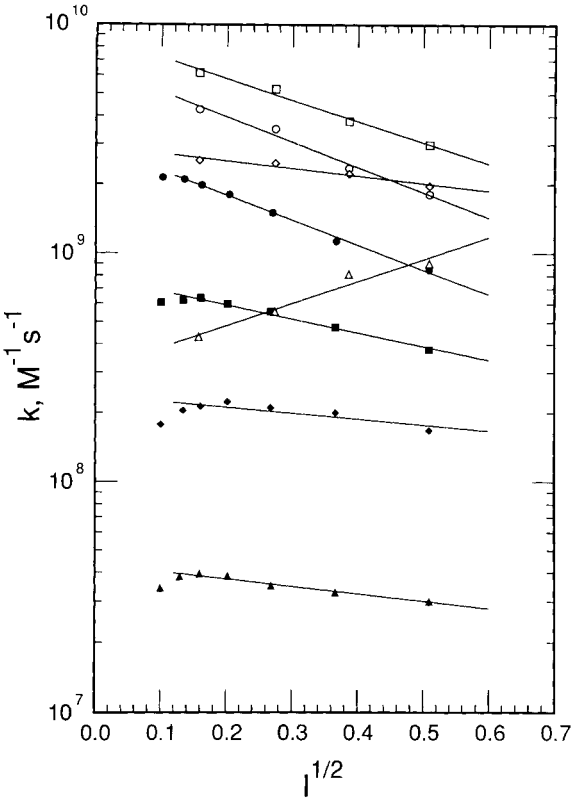

Fig. 4. Effect of ionic strength (I) on reaction rates as measured experimentally at pH 8 by pulse radiolysis (solid symbols) and computationally (open symbols) from Brownian dynamics simulations. Experimentally, the wild-type (●) enzyme, the most active, was most affected by ionic strength, R143K mutant (■) slightly less so, with R143I (◆) and R143E (▲) mutants affected very little. R143E was the least active of the group. Computationally, the ionic strength effects were similar to those determined experimentally, except in the case of the R143E mutant (△). The relative activities were less accurate; the R143K mutant (□) activity was calculated as greater than the wild-type (○), the R143I (◇) was also relatively high, and the activity of the R143E mutant was overestimated by over an order of magnitude.

tive SOD and three mutants of residue 143. (The $I^{1/2}$ term derives from the Debye–Hückel limit of the Brønsted–Bjerrum equation, $\log k = (z_- \times z_+)I^{1/2}$ + constant, where z_- and z_+ are the charges of the negative and positive ions.[37]) The wild-type enzyme showed a marked decrease in rate with increased ionic strength to the same degree observed previously in bovine SOD.[12] The R143K mutant demonstrated a similar behavior. In contrast, ionic strength changes at pH 8 affected the rate of the neutral and acidic mutants very little. These results confirm that a positive charge at 143 is critical in electrostatic recognition of and interactions with the superoxide substrate.

Although the exact charge on the enzyme cannot be derived quantitatively from the ionic strength dependence over the range of ionic strengths used in this work,[12] the slope of the line in Figure 4 still provides an empirical picture of the relative electrostatic attraction between SOD and superoxide.[10,38] From the experimental data, the apparent charge was most positive in the wild-type SOD; that of the R143K mutant was also significantly positive, but nearly halved. The apparent charges of the R143I on the enzyme and R143E mutants were even lower. Therefore an Arg at position 143 is necessary in order to obtain the highest electrostatic attraction to the superoxide substrate.

Reaction simulations with Brownian dynamics tested computational predictability of the ionic strength dependencies of the wild-type and mutant SODs, extending computational studies by Sines et al.[11] and Klapper et al.[39] Once the electrostatic potentials were calculated at four different ionic strengths (e.g., see Fig. 2), rate simulations for each protein at each ionic strength yielded the results shown in Figure 4. These results demonstrate that the calculations at varying ionic strengths were able to reproduce several of the log of rate versus ionic strength slopes fairly well, with differences within experimental error for the wild-type and R143I enzymes, and somewhat larger for the R143K mutant. In all cases, the calculated rates were higher than the experimental values, possibly due to the necessity of defining a reaction radius of 7.0 Å in order to avoid grid sampling errors in the narrow active site channel (see Fig. 1b).

The slope calculated for the Glu mutant did not match the experimental data in Figure 4, which was determined at pH 8. Instead, it was more representative of the mutant enzyme's behavior at ~pH 10 (see Fig. 6 and corresponding discussion below). The log of rate versus ionic strength slope is indicative of the dominance of the positively charged active site over the overall negative charge of the enzyme. In this instance, the UHBD calculations overestimated the influence of the negative charge and underestimated the effect of the active site positive charge on the enzyme's electrostatic potential (see Fig. 2), resulting in a computational system that is more favorably affected by higher ionic strengths than is found experimentally.

The relative activities of the calculated data were generally correct, although the Lys mutant was predicted to have a higher activity than the native SOD. Four possible explanations exist for this difference: (1) The protein is treated as a rigid body in the computational model, preventing the Lys ammonium group, which has a more focused positive charge than the Arg guanidinium, from moving. The positive charge of the Lys head group is therefore highly concentrated relative to the Arg in the calculation and has a greater long-range electrostatic effect on the simulated superoxide (see Fig. 5). (2) The Lys, which is likely not as rigidly held by hydrogen bonds as the Arg, may be conformationally mobile enough to block off the active site channel periodically. In addition, the position in which

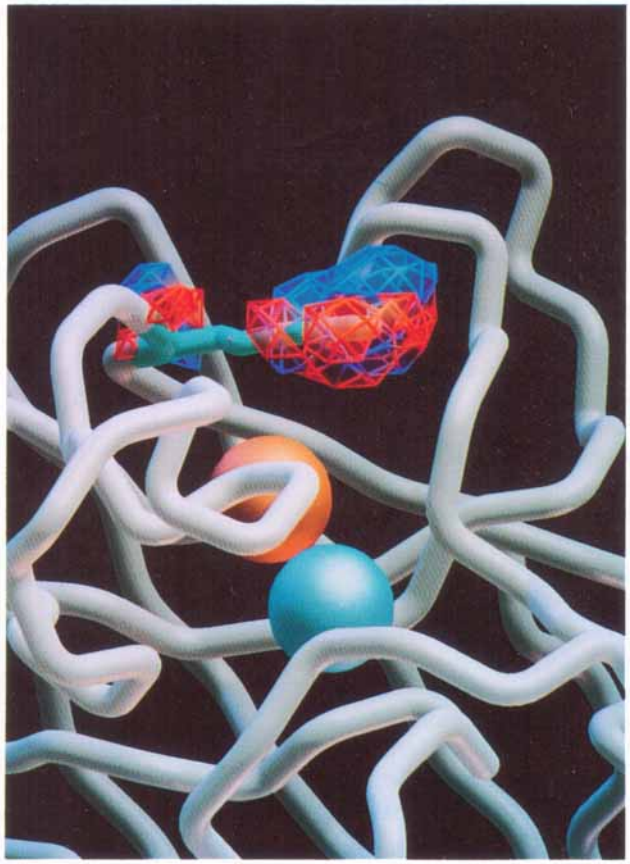

Fig. 5. Difference grid between the electrostatic potentials of the wild-type SOD and R143K mutant enzyme as calculated by the UHBD program, illustrating the specific local differences in the distribution of positive potential near the active site. Excess positive potential in the wild-type enzyme, which occurs directly adjacent to the superoxide binding site, is indicated by red shading. Excess positive potential in the Lys mutant, which occurs away from the superoxide binding site, is indicated by blue shading. The enzyme fold (white tubes) is shown with the Arg-143 side chain (blue tubes), the copper ion (orange sphere) and the zinc ion (blue sphere). Figure rendered with the program AVS,[41] with tubes generated by the module MCS TUBES (written by Y. Chen and A. Olson).

the Lys is placed in our simulations may not be the actual or optimal one. (3) The Lys was modeled solely as a positively charged side chain in our simulations, as a pH of 7 was assumed. As evidenced from the behavior of the mutant in the pH dependency studies, the enzyme is likely in a state of partial deprotonation in the sample at pH 8. Experimentally, though, the R143K mutant is still less active than the wild-type at low pH, making this unlikely to be the complete explanation for the higher activity, but a possible explanation for the higher discrepancy in the slope, which would be steeper at lower pH experimentally. (4) Long-range electrostatics is not the only factor at work in the system.

If Arg-143 strictly contributed to the long-range electrostatics of SOD alone, the computational results, which reflect such contributions, predict a 15-fold range in activity among the wild-type and mutant enzymes studied. Experimentally, however, a 50-fold difference was observed at pH 8 (Fig. 4). Comparisons of computational and experimental data showed a much closer match for mutations at other residues[22] (unpublished results) in which long-range electrostatic influence was the critical component of their contribution to enzyme activity.

As evidenced by the decrease in positive potential directly above the copper ion on replacement of Arg-143 with Lys (Fig. 5), Arg contributes to the local electrostatic environment necessary for binding superoxide and/or facilitating proton transfer from solvent. In addition, the guanidinium group of Arg-143 is rigidly held in place by several hydrogen bonds deep in the active site channel. Hydrogen bonds to one of the guanidinium's amino groups ideally orient the other amino group for interaction with bound superoxide. Collectively our results indicate that Arg-143 is therefore vital not only to the long-range electrostatics of SOD, but to local electrostatics and the enzyme mechanism as well.

pH versus Ionic Strength Dependencies of Enzyme Rates

The effect of pH on the dismutation rate at both high (0.2 M NaCl, 5 mM NaH_2PO_4, 10 mM $NaHCO_2$; $I^{1/2}$ = 0.46) and low (0.01 M $NaHCO_2$, 5 mM HEPES; $I^{1/2}$ = 0.1) ionic strengths were measured for the wild-type, R143K, and R143E enzymes (Fig. 6). All showed the typical drop in rate at ~pH 10 mentioned above at both ionic strengths. For the wild-type enzyme below pH 10.5, the rate was substantially lower at high ionic strengths due to damping of the attractive electrostatic forces between $O_2^{\cdot-}$ and the positively charged active site. At pH 10.5 and above, as Arg-143 was deprotonated, the overall negative charge of the enzyme overwhelmed any remaining positive charge at the active site. The high ionic strength solution then shielded incoming $O_2^{\cdot-}$ from the repulsive potential of the enzyme, resulting in an increase in activity relative to the low ionic strength solution. In the R143K mutant, deprotonation of Lys-143 began at ~pH 7.5, and by pH 8.5 any remaining positive charge at the active site was too weak to counteract the overall negative charge of the enzyme. Again, the high ionic strength increased the reaction rate at this point. The R143E mutant, in which Glu-143 was completely deprotonated by ~pH 7, began to demonstrate the effect of repulsive charge damping by high ionic strength at about pH 7.5.

Ionic strength effects at three different pH values were investigated as well for the R143K mutant (Fig. 7) as a verification of the changes in pH dependence of rate at low and high ionic strengths. At pH 6.52, the slope of the ionic strength dependence of the rate was −1.1 between $I^{1/2}$ values of 0.15 and 0.6, with a threefold drop in rate. At pH 8.0, the slope was less sharp at −0.64, with a drop of about twofold in rate. By pH 10.75, the slope, 0.34, showed an increase, rather than a decrease, of about 1.5 in rate with increasing ionic strength. These results confirmed those reported above: at high ionic strength and low pH there was a marked decrease in rate, at about pH 8, the effects of ionic strength were lessened considerably, and at high pH there was a reversal in ionic strength effects.

These two sets of experiments illustrate the ability of the R143K mutant to shuttle between the behaviors of an enzyme with a positively charged residue at position 143 and a neutralized or negatively charged one. The fact that this occurs near physiological pH is likely the primary reason that a Lys at position 143 is an unfavorable substitution in nature.

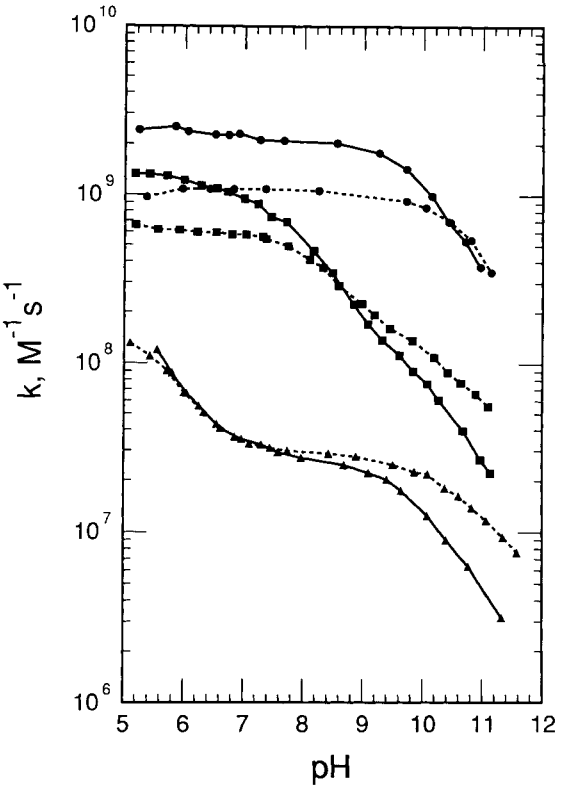

Fig. 6. Effect of ionic strength on pH dependence of reaction rate. The solid lines represent data at low ($I^{1/2}$ = 0.1) ionic strength, the dotted lines at high ($I^{1/2}$ = 0.46M) ionic strength. When the ionic strength was increased, the activity of the wild-type enzyme (●) decreased most at lower pH. At higher ionic strength, the R143K mutant activity (■) decreased at lower pH, but increased at higher pH, while the R143E mutant (▲) was unaffected at low pH but increased in activity at higher pH with an increase in ionic strength.

CONCLUSIONS

The results presented above establish that Arg-143 has a major electrostatic function in enhancing the activity of human Cu,Zn SOD. Of all variants tested, the wild-type Arg-143 enzyme had the highest dismutation rate; charge neutralization decreased the rate by 10-fold and charge reversal by 100-fold, the most dramatic charge dependence in a residue seen to date in our mutational studies. Arg-143 was also the most affected by ionic strength changes, and therefore appeared the most positive to an incoming superoxide substrate; the R143K mutant was influenced only about half as much.

The involvement of Arg-143 in capacities other than electrostatic guidance, however, is reflected in the inconsistencies between the computational and pulse radiolysis ionic strength dependencies of the wild-type and mutant enzyme rates. In contrast to the results presented here, we have found good correlation between experiment and computation for mutations at other residues in which electrostatics is likely the sole contribution the residue makes to enzymatic activity. The discrepancy between the calculated and observed rates for residue 143 mutants strongly suggests that an Arg at position 143 serves other purposes. This view is supported by sev-

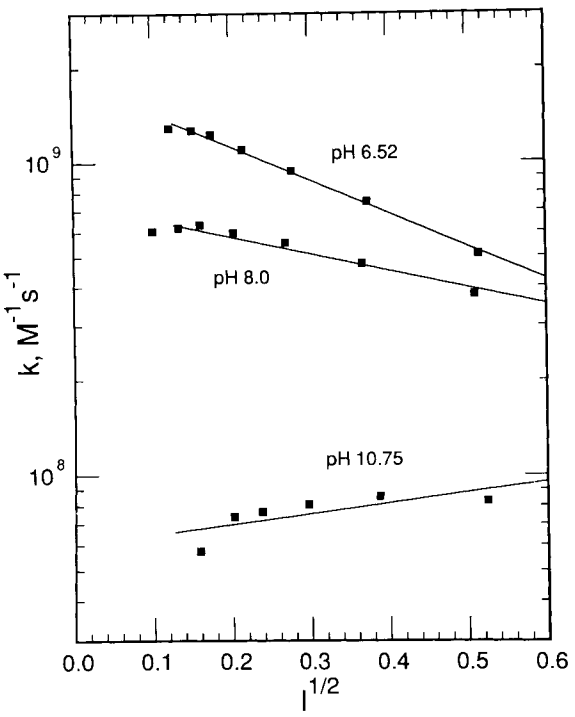

Fig. 7. Effect of pH on ionic strength dependence in R143K mutant enzyme. At pH 6.52, the mutant's activity is substantially decreased with increasing ionic strength. The decrease is less pronounced at pH 8.0, and the activity actually increases at pH 10.75.

eral observations: (1) the activity of the R143K mutant is lower than that of wild-type enzyme, (2) the local electrostatic potential above the active site becomes less positive on mutation to Lys, (3) the guanidinium group of Arg is ideally oriented as a docking point for the bound superoxide, and (4) the wild-type Arg-143 was less pH dependent, and thus had the same reaction rate over a greater pH range, than any of the charged mutants.

Overall, our results quantitatively define the electrostatic role for active site Arg-143 in enzymatic activity and attest to the residue's involvement in the mechanism of Cu,Zn SOD. The combined structural, computational, and biochemical results demonstrate that Arg-143 is critically positioned to provide a delocalized positive charge to both attract and stabilize the negatively charged superoxide substrate. No other standard amino acid is able to fulfill this role.

ACKNOWLEDGMENTS

We thank Michael Pique and Malcolm Davis for help in testing and altering the Brownian dynamics programs, Diane Bauer, Karin Imlay, and Irma Laria for expert technical assistance, and Michael Pique for assisting with the computer graphics. This work was supported by NIH Grant GM 39345 (J.A.T., R.A.H.), GM 37684 (E.D.G.), NSF Grant DIR 882385 (J.A.T., E.D.G.), NIH Fellowships GM 11612 and HL 07695 (C.L.F.), and by Chiron Corporation (R.A.H.) and by a grant from the Welcome Trust (R.A.H.). Brownian dynamics calculations used the computer resources at Scripps and additional computer time provided by Cray Research, Inc. Pulse radiolysis rate studies were supported by NIH Grant GM 23658 and carried out at Brookhaven National Laboratory, which is operated under contract DE-AC02-76CH00016 to the U.S. Dept. of Energy.

REFERENCES

1. Keller, G.-A., Warner, T.G., Steimer, K.S., Hallewell, R.A. Cu,Zn superoxide dismutase is a peroxisomal enzyme in human fibroblasts and hepatoma cells. Proc. Natl. Acad. Sci. U.S.A. 88:7381–7385, 1991.
2. Fridovich, I. Superoxide dismutases. In: "Advances in Enzymology," Vol. 58. Meister, A. ed. New York: John Wiley, 1986: 61–97.
3. Phillips, J.P., Campbell, S.D., Michaud, D., Charbonneau, M., Hilliker, A.J. A null mutation of cSOD in *Drosophila* confers hypersensitivity to paraquat and reduced longevity. Proc. Natl. Acad. Sci. U.S.A. 86:2761–2765, 1989.
4. Deng, H.-X., Hentati, A., Tainer, J.A., Iqbal, Z., Cayabyab, A., Hung, W.-Y., Getzoff, E.D., Hu, P., Herzfeldt, B., Roos, R.P., Warner, C., Deng, G., Soriano, E., Smyth, C., Parge, H.E., Ahmed, A., Roses, A.D., Hallewell, R.A., Pericak-Vance, M.A., Siddique, T. Amyotrophic lateral sclerosis and structural defects in Cu,Zn superoxide dismutase. Science 261:1047–1051, 1993.
5. Rosen, D.R., Siddique, T., Patterson, D., Figlewicz, D.A., Sapp, P., Hentati, A., Donaldson, D., Goto, J., O'Regan, J.P., Deng, H.-X., Rahmani, Z., Krizus, A., McKenna-Yasek, D., Cayabyab, A., Gaston, S.M., Berger, R., Tanzi, R.E., Halperin, J.J., Herzfeldt, B., den Bergh, R.V., Hung, W.-Y., Bird, T., Deng, G., Mulder, D.W., Smyth, C., Laing, N.G., Soriano, E., Pericak-Vance, M.A., Haines, J., Rouleau, G.A., Gusella, J.S., Horvitz, H.R., Brown, R.H. Jr. Mutations in Cu/Zn superoxide dismutase gene are associated with familial amyotrophic lateral sclerosis. Nature (London) 362:59–62, 1993.
6. Parge, H.E., Hallewell, R.A., Tainer, J.A. Atomic structures of wild-type and thermostable mutant recombinant human CuZn superoxide dismutase. Proc. Natl. Acad. Sci. U.S.A. 89:6109–6113, 1992.
7. Rotilio, G., Bray, R.C., Fielden, E.M. A pulse radiolysis study of superoxide dismutase. Biochim. Biophys. Acta 268:605–609, 1972.
8. Klug, D., Rabani, J., Fridovich, I. A direct demonstration of the catalytic action of superoxide dismutase through the use of pulse radiolysis. J. Biol. Chem. 247:4839–4842, 1972.
9. Cudd, A., Fridovich, I. Electrostatic interactions in the reaction mechanism of bovine erythrocyte superoxide dismutase. J. Biol. Chem. 257:11443–11447, 1982.
10. Argese, E., Viglino, P., Rotilio, G., Scarpa, M., Rigo, A. Electrostatic control of the rate-determining step of the copper, zinc superoxide dismutase catalytic reaction. Biochemistry 26:3224–3228, 1987.
11. Sines, J.J., Allison, S.A., McCammon, J.A. Point charge distributions and electrostatic steering in enzyme/substrate encounter: Brownian dynamics of modified copper/zinc superoxide dismutases. Biochemistry 29:9403–9412, 1990.
12. McAdam, M.E. A consideration of the effects of added solutes on the activity of bovine superoxide dismutase. Biochem. J. 161:697–699, 1977.
13. Tainer, J.A., Getzoff, E.D., Beem, K.M., Richardson, J.S., Richardson, D.C. Determination and analysis of the 2Å structure of copper, zinc superoxide dismutase. J. Mol. Biol. 160:181–217, 1982.
14. Tainer, J.A., Getzoff, E.D., Richardson, J.S., Richardson, D.C. Structure and mechanism of copper, zinc superoxide dismutase. Nature (London) 306:284–287, 1983.
15. Malinowski, D.P., Fridovich, I. Chemical modification of

arginine at the active site of the bovine erythrocyte superoxide dismutase. Biochemistry 18:5909–5917, 1979.
16. Borders, C.L. Jr., Johansen, J.T. Identification of Arg-143 as the essential arginyl residue in yeast Cu,Zn superoxide dismutase by use of a chromophoric arginine reagent. Biochem. Biophys. Res. Commun. 96:1071–1078, 1980.
17. Borders, C.L. Jr., Saunders, J.E., Blech, D.M., Fridovich, I. Essentiality of the active-site arginine residue for the normal catalytic activity of Cu,Zn superoxide dismutase. Biochem. J. 230:771–776, 1985.
18. Paci, M., Desideri, A., Sette, M., Rotilio, G. NMR evidence for perturbation of the copper coordination sphere upon chemical modification of arginine 141 in bovine Cu,Zn superoxide dismutase. Arch. Biochem. Biophys. 286:222–225, 1991.
19. Beyer, W.F. Jr., Fridovich, I., Mullenbach, G.T., Hallewell, R.A. Examination of the role of arginine-143 in the human copper and zinc superoxide dismutase by site-specific mutagenesis. J. Biol. Chem. 262:11182–11187, 1987.
20. Getzoff, E.D., Tainer, J.A., Stempien, M.M., Bell, G.I., Hallewell, R.A. Evolution of CuZn superoxide dismutase and the Greek key β-barrel structural motif. Proteins 5:322–336, 1989.
21. Getzoff, E.D., Tainer, J.A., Weiner, P.K., Kollman, P.A., Richardson, J.S., Richardson, D.C. Electrostatic recognition between superoxide and copper, zinc superoxide dismutase. Nature (London) 306:287–290, 1983.
22. Getzoff, E.D., Cabelli, D.E., Fisher, C.L., Parge, H.E., Viezzoli, M.S., Banci, L., Hallewell, R.A. Faster superoxide dismutase mutants designed by enhancing electrostatic guidance. Nature (London) 358:347–351, 1992.
23. Hallewell, R.A., Laria, I., Tabrizi, A., Carlin, G., Getzoff, E.D., Tainer, J.A., Cousens, L.S., Mullenbach, G.T. Genetically engineered polymers of human CuZn superoxide dismutase. J. Biol. Chem. 264:5260–5268, 1989.
24. Lepock, J.R., Frey, H.E., Hallewell, R.A. Contribution of conformational stability and reversibility of unfolding to the increased thermostability of human and bovine superoxide dismutase mutated at free cysteines. J. Biol. Chem. 265:21612–21618, 1990.
25. Steinman, H. Bacteriocuprein superoxide dismutase of *Photobacterium leiognathi*. Isolation and sequence of the gene and evidence for a precursor form. J. Biol. Chem. 262:1882–1887, 1987.
26. Farabaugh, P.J. Sequence of the *lacI* gene. Nature (London) 274:765–769, 1978.
27. Hallewell, R.A., Masiarz, F.R., Najarian, R.C., Puma, J.P., Quiroga, M.R., Randolph, A., Sanchez-Pescador, R., Scandella, C.J., Smith, B., Steimer, K.S., Mullenbach, G.T. Human Cu/Zn superoxide dismutase cDNA: Isolation of clones synthesising high levels of active or inactive enzyme from an expression library. Nucleic Acids Res. 13: 2017–2034, 1985.
28. Hallewell, R.A., Imlay, K.C., Lee, P., Fong, N.M., Gallegos, C., Getzoff, E.D., Tainer, J.A., Cabelli, D.E., Tekamp-Olson, P., Mullenbach, G.T., Cousens, L.S. Thermostabilization of recombinant human and bovine CuZn superoxide dismutases by replacement of free cysteines. Biochem. Biophys. Res. Commun. 181:474–480, 1991.
29. Cabelli, D.E., Bielski, B.H. Kinetics and mechanism for the oxidation of ascorbic acid/ascorbate by HO_2/O_2^- radicals. A pulse radiolysis and stopped-flow photolysis study. J. Phys. Chem. 87:1809–1812, 1983.
30. Schwarz, H.A. Free radicals generated by radiolysis of aqueous solutions. J. Chem. Ed. 58:101–105, 1981.
31. Banci, L., Carloni, P., Penna, G.L., Orioli, P.L. Molecular dynamics studies on superoxide dismutase and its mutants: The structural and functional role of Arg 143. J. Am. Chem. Soc. 114:6994–7001, 1992.
32. Davis, M.E., McCammon, J.A. Electrostatics in biomolecular structure and dynamics. Chem. Rev. 90:509–521, 1990.
33. Weiner, S.J., Kollman, P.A., Case, D., Singh, U.C., Ghio, C., Alagona, G., Profeta, S. Jr., Weiner, P. A new force field for molecular mechanical simulation of nucleic acids and proteins. J. Am. Chem. Soc. 106:765–784, 1984.
34. Geysen, H.M., Tainer, J.A., Rodda, S.J., Mason, T.J., Alexander, H., Getzoff, E.D., Lerner, R.A. Chemistry of antibody binding to a protein. Science 235:1184–1190, 1987.
35. Banci, L., Cabelli, D.E., Getzoff, E.D., Hallewell, R.A., Viezzoli, M.S. An essential role for the conserved Glu-133 in the anion interaction with superoxide dismutase. J. Inorg. Biochem. 50:89–100, 1993.
36. Banci, L., Bertini, I., Luchinat, C., Hallewell, R.A. An investigation of superoxide dismutase Lys-143, Ile-143, and Glu-143 mutants: Cu_2Co_2SOD derivatives. J. Am. Chem. Soc. 110:3629–3633, 1988.
37. Castellan, G.W. Physical chemistry. 2 Ed. Reading: Addison-Wesley. 1971: 787–789.
38. Alberty, R.A., Hammes, G.G. Application of the theory of diffusion-controlled reactions to enzyme kinetics. J. Phys. Chem. 62:154–159, 1958.
39. Klapper, I., Hagstrom, R., Fine, R., Sharp, K., Honig, B. Focusing of electric fields in the active site of Cu-Zn superoxide dismutase: Effects of ionic strength and amino-acid modification. Proteins 1:47–59, 1986.
40. Carson, M. Ribbon models of macromolecules. J. Mol. Graph. 5:103–106, 1987.
41. Upson, C., Faulhaber, T. Jr., Kamins, D., Laidlaw, D., Schlegel, D., Vroom, J., Gurwitz, R., van Dam, A. The Application Visualization System: A computational environment for scientific visualization. IEEE Comp. Graph. Appl. 9:30–42, 1989.